Journal of the European Ceramic Society 21 (2001) 719–726

www.elsevier.com/locate/jeurceramsoc

An X-ray study of the trimetallic $La_xSm_{1-x}FeO_3$ orthoferrites

Luigi Sangaletti [a,*], Laura E. Depero [b], Brigida Allieri [b], Patrizia Nunziante [c], Enrico Traversa [c]

[a] *Istituto Nazionale per la Fisica della Materia (INFM) and Dipartimento di Matematica e Fisica, Università Cattolica del Sacro Cuore, Via Trieste 17, 25121 Brescia, Italy*

[b] *Istituto Nazionale per la Fisica della Materia (INFM) and Dipartimento di Ingegneria Meccanica, Università di Brescia, Via Branze 38, 25123 Brescia, Italy*

[c] *Consorzio Interuniversitario Nazionale per la Scienza e Tecnologia dei Materiali (INSTM) and Dipartimento di Scienze e Tecnologie Chimiche, Universita' di Roma "Tor Vergata", 00133 Roma, Italy*

Received 19 May 2000; received in revised form 6 September 2000; accepted 10 September 2000

Abstract

The structural properties of the $La_xSm_{1-x}FeO_3$ trimetallic orthoferrites are described on the basis of a Rietveld analysis of X-ray diffraction pattern. Ultrafine powders of these oxides are prepared by the thermal decomposition at low temperatures of the corresponding hexacyanocomplexes. Single-phase compounds are obtained. Their structural parameters can be tuned by properly changing the Sm/La stoichiometric ratio. © 2001 Elsevier Science Ltd. All rights reserved.

Keywords: Ferrites; (La,Sm)FeO_3; Powders-chemical preparation; Perovskites; X-ray methods

1. Introduction

Due to their peculiar magnetic properties, rare-earth orthoferrites $LnFeO_3$ with perovskite-type structure are still attracting much attention; considerable efforts are being done to elucidate the origin of the weak ferromagnetism and spin-orientation transitions which occur in most of the $LnFeO_3$ series compounds.[1–3]

From a technological point of view, rare-earth orthoferrites are very interesting materials for a wide range of electroceramic applications. In fact, these materials are known to display ionic and electronic defects,[4] which are the cause of their mixed conductivity.[5,6] Thus, these oxides are important candidates for the development of solid oxide fuel cells,[7] oxygen-permeation membranes[8,9] for conversion of methane to syngas,[10] gas-diffusion electrodes,[11] electrode materials for oxygen sensors[12,13] active catalysts for oxidation[14] or reduction of pollutant gases[15] and of magneto–optical sensors. Moreover, they can be used as active materials for chemical sensors, for the detection of various vapours[16,17] and gases,[18–24] showing the most promising results for the detection of NO_2[25–27] in thick-film prototype sensors which have been applied for environmental monitoring field tests.[28,29]

In a previous paper, we have reported the synthesis of the $La_xSm_{1-x}FeO_3$ trimetallic orthoferrites and their structural characterization, together with a Raman scattering study.[30] Ultrafine powders of these oxides have been prepared by the thermal decomposition at low temperatures of the corresponding hexacyanocomplexes.[31] In this study, the structural properties of the $La_xSm_{1-x}FeO_3$ orthoferrites are described on the basis of a Rietveld analysis of X-ray diffraction pattern. It was found that the structural parameters can be tuned by properly changing the Sm/La stoichiometric ratio. A comparison with the structural parameters reported previously in the literature for similar compounds (bimetallic rare-earth orthoferrites) in single crystal[32] is also discussed.

2. Experimental

2.1. Sample preparation

Trimetallic orthoferrites have been prepared starting from $La_xSm_{1-x}[Fe(CN)_6].\ nH_2O$ ($x = 0$, 0.2, 0.4, 0.6, 0.8, and 1) heteronuclear complexes.[30] These complexes were

* Corresponding author.
E-mail address: Sangalet@dmf.les.unicatt.it (L. Sangaletti).

PII: S0955-2219(00)00267-3

synthesized at room temperature by mixing aqueous solutions of appropriate amounts of $La(NO_3)_3{\cdot}6H_2O$, $Sm(NO_3)_3{\cdot}6H_2O$, and $K_3Fe(CN)_6$. After the mixtures were stirred at room temperature for 30 min, the precipitate obtained was collected by suction filtration and then washed with water, ethanol and diethyl ether, before drying in air at 50°C. Atomic absorption analysis showed that the potassium content of the purified complexes was lower than 0.05 wt.%. The complexes were decomposed at a rate of 5°C/min in air up to 1000°C to obtain the trimetallic orthoferrites in the series $La_xSm_{1-x}FeO_3$.

2.2. X-ray diffraction

All the diffraction experiments were carried out at room temperature with a Philips MPD 1830 automated powder diffractometer, equipped with graphite-monochromated CuK_α radiation in the Bragg–Brentano parafocusing geometry.

On the basis of the XRD data a Rietveld analysis was carried out by using the Rietveld code included into the Cerius^2 simulation package.[33]

3. Results and discussion

3.1. Description of the crystal structure and Rietveld analysis

The rare earth orthoferrites crystallize as perovskite-type structures with orthorhombic distortion. In the ideal cubic ABO_3 perovskite structure the A cations are surrounded by 12 equidistant oxygen ions, whereas the B cations present an octahedral coordination with oxygen. A Rietveld analysis of X-ray diffraction patterns of bimetallic single crystals of $LnFeO_3$ has been performed by Marezio et al.[32] These data will be used as a reference throughout the present study on the trimetallic $La_xSm_{1-x}FeO_3$ perovskites.

Fig. 1 shows the XRD patterns of the $La_xSm_{1-x}Fe$-complexes decomposed at 1000°C. All the observed XRD patterns show sharp reflections. This indicates that, in spite of the La substitution with Sm, ordered structures are formed for all the mixed La and Sm phases. No reflections from superstructure have been detected. Therefore, a random distribution of La and Sm in the cation sites was assumed.

Some disorder effect in the anion sublattice is expected because the coordination of La with oxygen is slightly different from the coordination of Sm with oxygen. Unfortunately, this disorder could not be detected by XRD due to the weak contribution of oxygen ions to the structure factors.

As the La content, x, increases, the orthorhombic distortion of the unit cell decreases.[30] Indeed, the larger

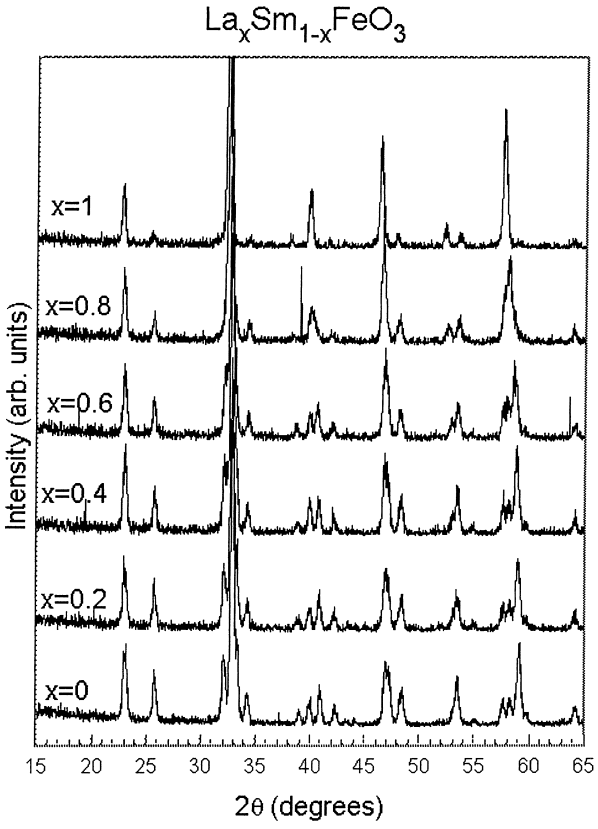

Fig. 1. XRD patterns of the $La_xSm_{1-x}FeO_3$ orthoferrites.

the La content, the weaker the intensity of the manifold of peaks around the most intense XRD reflections.

On the basis of the XRD data a Rietveld analysis was carried out by using the Rietveld code included into the Cerius^2 simulation package.[33]

In the Rietveld refinement, the $SmFeO_3$ structure (ICSD Card Nr.27276) was assumed as the starting point. The other structures ($La_{1-x}Sm_xFeO_3$) were refined by progressively substituting the Sm cation with La and assuming the nominal stoichiometry values $x = 1$, 0.8, 0.6, 0.4, 0.2, 0.0. The Rietveld analysis was performed on the experimental data collected in a 7.00–64.8° 2θ range. In addition to the cell parameters, the following parameters were also refined:

- background (three parameters)
- vertical (rigid) displacement (one parameter)
- profile (five parameters) + asymmetry (one parameter)
- overall thermal factor
- all the atomic coordinates.

Finally, in the A cation site the Sm ion was set and the site occupancy was refined to account for the substitution of Sm with the La cation, which has a lower atomic number Z. Attempts to refine the data by using different thermal factors for different atoms yielded worse R-factors.

Table 1

(a) Results of the Rietveld refinement for $SmFeO_3$

$SmFeO_3$

	$a = 5.3978(4)$	$b = 5.5917(5)$	$c = 7.7059(7)$	
	x	*y*	*z*	Occupancy
Sm	0.9853(5)	0.0555(3)	0.25	1.013(6)
O	0.697(3)	0.301(2)	0.045(2)	1
O	0.092(3)	0.474(3)	0.25	1
Fe	0	0.5	0	1
	Temp. factor	R–P	R–WP	
	1.75(8)	6.7	9.29	

(b) Results of the Rietveld refinement for $La_{0.2}Sm_{0.8}FeO_3$

$La_{0.2}Sm_{0.8}FeO_3$

	$a = 5.4079(4)$	$b = 5.5887(4)$	$c = 7.7158(6)$	
	x	*y*	*z*	Occupancy
Sm/La	0.9857(6)	0.0541(4)	0.25	1.002(7)
O	0.693(4)	0.304(3)	0.048(2)	1
O	0.086(4)	0.469(4)	0.25	1
Fe	0	0.5	0	1
	Temp. factor	R–P	R–WP	
	1.78(9)	8.61	13.22	

(c) Results of the Rietveld refinement for $La_{0.4}Sm_{0.6}FeO_3$

$La_{0.4}Sm_{0.6}FeO_3$

	$a = 5.4217(6)$	$b = 5.5866(7)$	$c = 7.729(1)$	
	x	*y*	*z*	Occupancy
Sm/La	0.9892(7)	0.0511(4)	0.25	1.013(7)
O	0.708(4)	0.294(3)	0.046(3)	1
O	0.100(5)	0.474(4)	0.25	1
Fe	0	0.5	0	1
	Temp. factor	R–P	R–WP	
	1.9(1)	9.0	13.38	

(d) Results of the Rietveld refinement for $La_{0.6}Sm_{0.4}FeO_3$

$La_{0.6}Sm_{0.4}FeO_3$

	$a = 5.4415(7)$	$b = 5.5813(8)$	$c = 7.749(1)$	
	x	*y*	*z*	Occupancy
Sm/La	0.9876(7)	0.0495(4)	0.25	0.988(7)
O	0.711(4)	0.297(3)	0.042(3)	1
O	0.088(6)	0.472(3)	0.25	1
Fe	0	0.5	0	1
	Temp. factor	R–P	R–WP	
	1.6(1)	8.25	13.38	

(e) Results of the Rietveld refinement for $La_{0.8}Sm_{0.2}FeO_3$

$La_{0.8}Sm_{0.2}FeO_3$

	$a = 5.492(1)$	$b = 5.571(1)$	$c = 7.810(2)$	
	x	*y*	*z*	Occupancy
Sm/La	0.992(1)	0.0420(5)	0.25	0.955(8)
O	0.696(5)	0.292(5)	0.043(4)	1
O	0.073(8)	0.483(5)	0.25	1
Fe	0	0.5	0	1
	Temp. factor	R–P	R–WP	
	1.8(1)	11.56	16.71	

(f) Results of the Rietveld refinement for La FeO_3

La FeO_3

	$a = 5.552(1)$	$b = 5.563(1)$	$c = 7.843(2)$	
	x	*y*	*z*	Occupancy
La	0.993(1)	0.0297(4)	0.25	0.924(7)
O	0.719(9)	0.302(6)	0.029(5)	1
O	0.08(1)	0.485(4)	0.25	1
Fe	0	0.5	0	1
	Temp. factor	R–P	R–WP	
	1.5(1)	9.47	15.33	

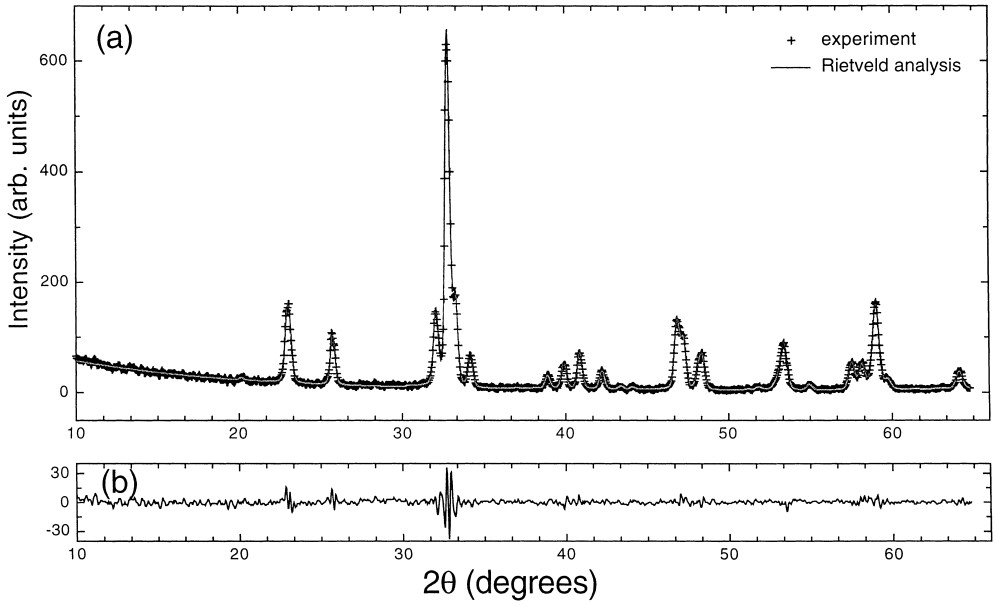

Fig. 2. Observed (+) and calculated (continuous line) profiles for $SmFeO_3$ (a). Difference between the observed and the calculated profile (b).

The intensity ratio among the different reflections was as it would be expected from the pattern calculated on the basis of the structural parameters reported in the single crystal database.[34] Provided that in the present case preferred orientation effects can be excluded, the measured ratio among the observed intensities indicates that the cation planes are mostly stoichiometric, because a relevant deviation from the calculated intensity can be assumed as a deviation from the expected cation stoichiometry.

The main results of the Rietveld analysis are reported in Table 1a–f. As an example of the Rietveld results, Fig. 2a shows the observed (+) and calculated (Rietveld; continuous line) XRD patterns for $SmFeO_3$. The difference between the observed and the calculated patterns is also shown in Fig. 2b.

As stated above, in the Rietveld analysis the occupation of the Ln lattice site has also been refined. As expected, the occupancy of the Ln^{3+} site increases with increasing x. Assuming that, far from absorption edges, the X-ray scattering factor scales with the atomic number Z, the occupancy of the Ln^{3+} site can also be calculated from the nominal stoichiometry. This value is reported in Table 2 as Z_{eff}/Z_{Sm} where $Z_{eff}=Z_{La}(1-x)+Z_{Smx}$. Given the small difference between the scattering factors of Sm and La, one can observe a good agreement between the nominal values and those obtained by the Rietveld analysis.

3.2. Lattice parameters

The calculated values of the lattice parameters as a function of the unit cell volume are shown in Fig. 3. The distortion in the basal plane of the orthorhombic unit cell increased with increasing the cell volume (i.e. with "x" in $La_xSm_{1-x}FeO_3$).

It is rather interesting to plot the lattice parameter dependence from the unit cell volume also for the whole family of $LnFeO_3$ orthoferrites investigated by Marezio et al.,[32] though it must be kept in mind that those data were obtained for single crystals prepared at high temperatures. From the data of Fig. 4a,b one can observe that in the parameter range between La and Sm a linear behavior is found also for the dimetallic compounds, while deviations from linearity are observed for rare earths heavier than Sm. Within this frame, the trimetallic La–Sm–Fe orthoferrites are single phase with structural parameters that vary linearly and can be tailored by a proper mixing of Sm and La.

Interesting information can also be obtained from the analysis of the dependence of the structural parameters on the Ln ionic radius. In the case of trimetallic orthoferrites, an effective ionic radius has to be defined as follows:[30]

$$r_{eff} = xr_{La} + (1-x)r_{Sm}$$

Table 2
Occupancy of the Ln^{3+} sites

x in $La_{1-x}Sm_xO_3$	Ln^{3+} occupancy from Rietveld	Ln^{3+} occupancy from Rietveld (normalized to Sm)	Z_{eff}/Z_{Sm}
1	0.92	0.91	0.919
0.8	0.96	0.94	0.935
0.6	0.99	0.98	0.952
0.4	1.01	1.00	0.968
0.2	1.00	0.99	0.984
0.0	1.01	1	1

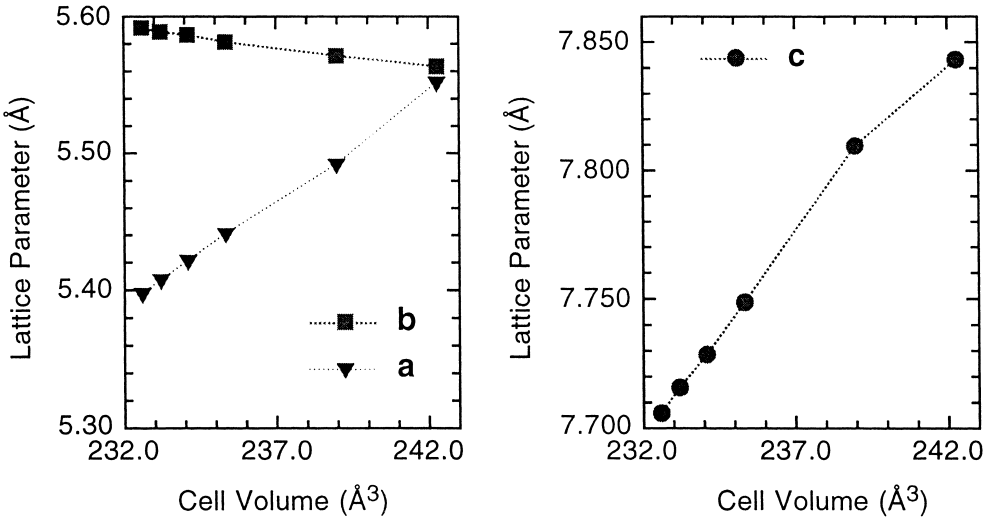

Fig. 3. Unit cell parameters (**a**, **b**, and **c**) vs cell volume.

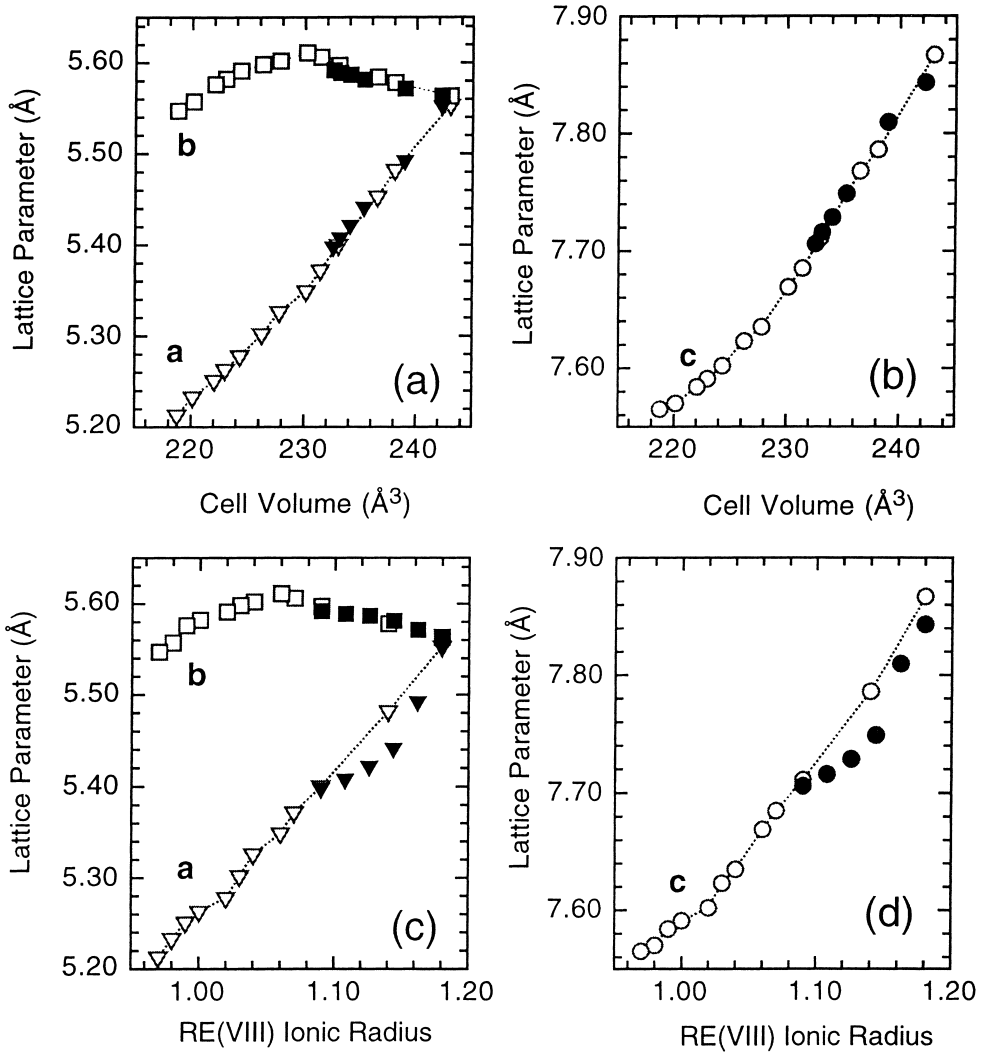

Fig. 4. Lattice parameter vs unit cell volume (3*a* and 3*b*) and effective RE (VIII) ionic radius (3*c* and 3*d*). Closed symbols: data of the present work, open symbols: data from Ref. 32 and 37.

where the r_{La} and r_{Sm} are the RE(VIII) ionic radii of La and Sm, respectively, as reported by Shannon and Prewitt.[35,36]

As shown in Fig. 4c,d, the relationship between the effective RE(VIII) ionic radius and cell parameter is slightly deviating from linearity for the values of *b* and *c* axis. This behavior can be interpreted as a Sm overstoichiometry with respect to the nominal value, as already observed for similar compounds prepared in the same way.[31] Therefore, if one assumes that the effective ionic radius is a well defined parameter, deviation from the expected linear behavior can be an index of the stoichiometry ratio between rare earths. In the present case, the results of Table 2 shows that the calculated effective *Z* number is usually higher than that expected from the nominal stoichiometry, which is in agreement with the observed deviation from linearity in Fig. 4.

3.3. Ln–O co-ordination

Due to the orthorhombic distortion, the 12 oxygen polyhedron around the A cations becomes quite distorted and the A–O distances vary over a large range. In fact, eight first-nearest neighbors and four-second nearest neighbors can be distinguished among the 12 rare-earth–oxygen distances. This is also the case of the compounds in the $La_{1-x}Sm_xFeO_3$ series where the eight first-nearest neighbor distances resulted to range from 2.32 to 2.76 Å while the four-second nearest neighbor distances range from 3.06 to 3.48 Å (Fig. 5).

3.4. Fe–O co-ordination: from 2+2+2 in $LaFeO_3$ to 4+2 in $SmFeO_3$

The distortion of the iron octahedra in the ABO_3 orthoferrites is known to be rather small even for the heavier RE such as Lu.[32] However, the present data (Fig. 6) indicate that a trend in the distortion can be observed as one changes the La content "*x*" in the compounds of the $La_{1-x}Sm_xFeO_3$ series. The analysis of the Rietveld results show that the Fe–O co-ordination can be described as a continuous variation from the 2+2+2 in $LaFeO_3$ to the 4+2 in $SmFeO_3$ and that the largest distortion is observed for the $LaFeO_3$ sample (Fig. 6).

However, X-ray diffraction patterns calculated on the basis of the Rietveld refinement results are almost identical to those calculated on the basis of the study of Marezio and Dernier,[37] and only minor differences in the intensity of very weak reflections were observed, which can be overshadowed by the experimental errors (Fig. 7). Therefore the results on the oxygen position refinement can be assumed as preliminary and further investigation by neutron diffraction should be carried out to make a final assesment on the oxygen position within the unit cell. Nevertheless, the observed behavior seems to be consistent with the increase of the average cation size with "*x*". Indeed, one can observe that the minor distortion in the Fe octahedron is found for smaller RE's (Sm). This indicates that the polyhedron around Sm does not affect to a large extent the Fe–O coordination, while when La is considered, the increase of the RE polyhedron size may increase the distortions on the oxygen cage around Fe. As expected, the difference between the first and second nearest-neighbor (NN) distances in the RE co-ordination polyhedron decreases as the RE cation size increases (Fig. 5).

3.5. Fe–O–Fe angle and superexchange

Rather important are also the Fe–O–Fe angles, since the orthoferrites exhibit magnetic properties that depend strongly on the effects of directional chemical bonding. The unit cell contains four Fe sites and four rare-earth sites that are equivalent for symmetry. Magnetic ordering

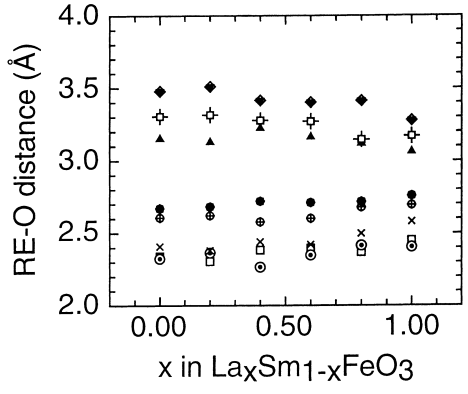

Fig. 5. Distribution of the RE–O distances as a function of the Lanthanum content "*x*" in $La_xSm_{1-x}FeO_3$.

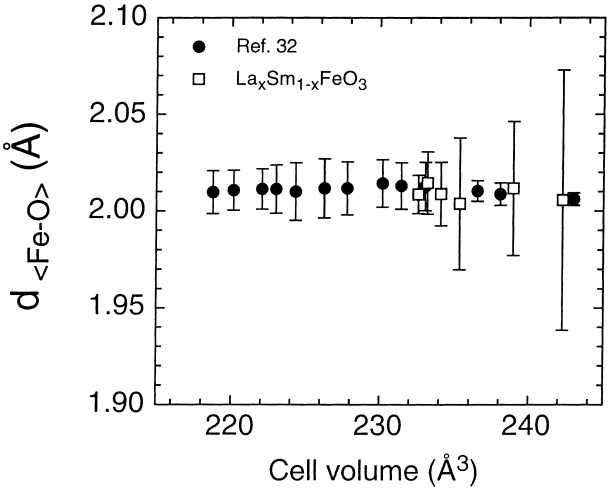

Fig. 6. Average Fe–O distance in the FeO_6 octahedron as a function of the Lanthanum content "*x*" in $La_xSm_{1-x}FeO_3$. The vertical bars indicate the deviation from the average value. Open symbols: present samples; closed symbols: data from Ref. 32 and 37.

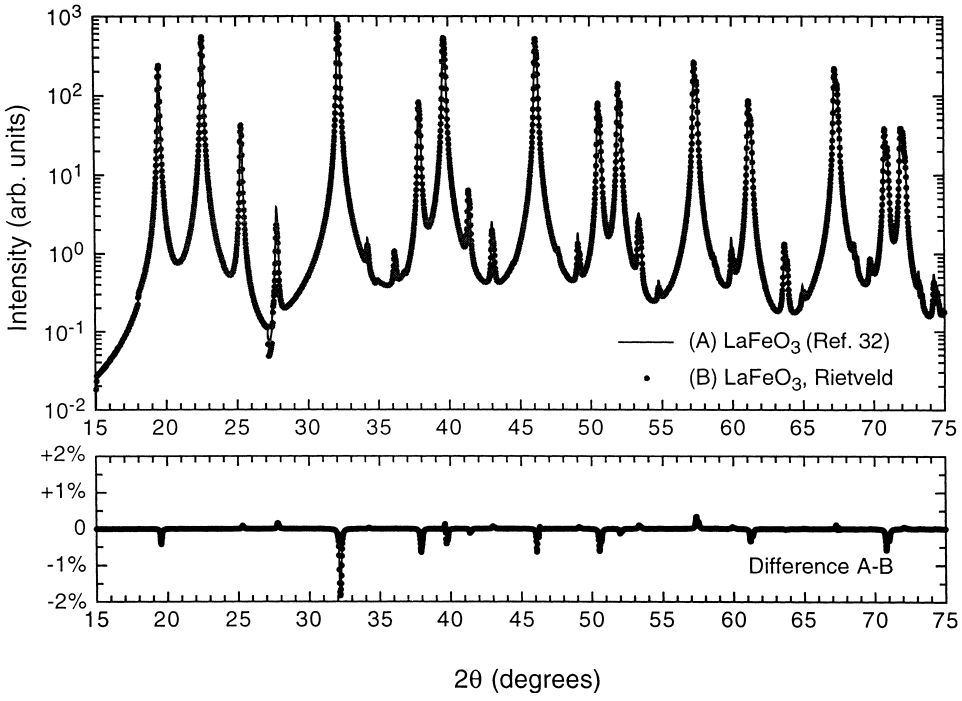

Fig. 7. Comparison between the present data and those calculated from the structural parameters refined by Marezio et al..[37].

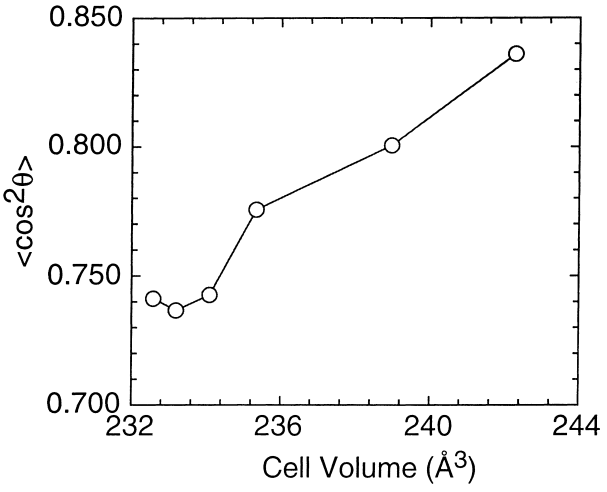

Fig. 8. Average squared cosine $<\cos^2\theta>$ of the Fe–O-Fe angles vs cell volume.

can make this sites inequivalent and give rise to four distinct Fe sublattices.[38] The orthoferrites are canted antiferromagnets with high transition temperatures that monotonically decrease as the rare-earth atomic number increases. The magnetic ordering involves primarily the Fe^{3+} ions that undergo superexchange interactions via Fe^{3+}–O^{2-}–Fe^{3+} bonds. The larger overlap of electron orbitals, which results from larger Fe–O–Fe bond angles, gives rise to correspondingly larger superexchange interactions and therefore higher transition temperatures T_N. Therefore the Neel temperature, which is proportional to the exchange constant, changes linearly with the average cosine-squared of the Fe–O–Fe bond angle.

From the present data, the values of the angle for $LaFeO_3$ (157.14°, 155.27°) and $SmFeO_3$ (149.25°, 149.75°) are in agreement with those reported in literature, while the angles found for the mixed compounds lay between those of two dimetallic compounds (Fig. 8). Therefore the highest value of the transition temperature is expected for $LaFeO_3$ and the lowest for $SmFeO_3$. The partial substitution of La with Sm is expected to decrease the Neel temperature until the lowest value is reached with total substitution of La with Sm.

4. Conclusions

An X-ray study of the trimetallic $La_xSm_{1-x}FeO_3$ orthoferrites has been carried out. It is shown that the compounds in this family are single phase with a random distribution of La and Sm in the cation sites. From a structural point of view the compounds obtained fit well into the series of $LnFeO_3$ orthoferrites, systematically studied by Marezio et al., on the basis of XRD data from single untwinned crystals.[32] The present samples provide a nearly-continuous variation of structural parameters between La and Sm. It was found that the structural parameters can be tuned by properly changing the Sm/La stoichiometric ratio. This achievement can disclose interesting routes to tune other physical properties, such as the energy of the magnetic interaction, by choosing the proper stoichiometry. Indeed, the Fe–O–Fe bond angle shows a monotonic increase with the effective RE mass, which should, consequently, induce an increase of the Neel temperature.

Acknowledgements

The present work was partly supported by the National Research Council of Italy (CNR), under the auspices of the Targeted Project "Special Materials for Advanced Technology II" (MSTA 2).

References

1. Maslen, E. N. and Spadaccini, N., *Acta Cryst*., 1993, **A49**, 661–667.
2. Streltsov, V. A., Ishizawa, N. and Kishimoto, S., *J. Synchrotron Radiation*, 1998, **5**, 1309–1316.
3. Streltsov, V. A. and Ishizawa, N., *Acta Cryst*., 1999, **B55**, 1–7.
4. Cherry, M., Islam, M. S. and Catlow, C. R. A., *J. Solid State Chem*., 1995, **118**, 125–132.
5. Wachsman, E. D., Oxide-ion conducting ceramics: defect chemistry and applications. In *Progress in Ceramic Basic Science: Challenge Toward the 21st Century*, ed. T. Hirai, S. I. Hirano and Y. Takeda. The Ceramic Society of Japan, Tokyo, Japan, 1996, pp. 129–143.
6. Stevenson, J. W., Armstrong, T. R., Carneim, R. D., Pederson, L. R. and Weber, W. J., *J. Electrochem. Soc*., 1996, **143**, 2722–2729.
7. Minh, N. Q., *J. Am. Ceram. Soc*., 1993, **76**, 563–588 (and references cited therein).
8. Teraoka, Y., Nobunaga, T. and Yamazoe, N., *Chem. Lett*., 1988, 503–506
9. Bouwmeester, H. J. M., Kruidhof, H. and Burggraaf, A. J., *Solid State Ionics*, 1994, **72**, 185–194.
10. Balachandran, U., Dusek, J. T., Sweeney, S. M., Poeppel, R. B., Mieville, R. L., Maiya, P. S., Kleefisch, M. S., Pei, S., Kobylinski, T. P., Udovich, C. A. and Bose, A. C., *Am. Ceram. Soc. Bull*., 1995, **74**(1), 71–75.
11. Karlsson, G., *Electrochim. Acta*, 1985, **30**, 1555–1561.
12. Inoue, T., Seki, N., Eguchi, K. and Arai, H., *J. Electrochem. Soc*., 1990, **137**, 2523–2527.
13. Alcock, C. B., Doshi, R. C. and Shen, Y., *Solid State Ionics*, 1992, **51**, 281–289.
14. McCarty, J. G. and Wise, H., *Catalysis Today*, 1990, **8**, 231–248.
15. Tabata, K. and Misono, M., *Catalysis Today*, 1990, **8**, 249–261.
16. Obayashi, H. and Kudo, T., *Nippon Kagaku Kaishi*, 1980, 1568–1572.
17. Shimizu, Y., Shimabukuro, M., Arai, H. and Seiyama, T., *Chem. Lett*., 1985, 917–920.
18. Li, W. B., Yoneyama, H. and Tamura, H., *Nippon Kagaku Kaishi*, 1982, 761–767.
19. Takahashi, Y. and Taguchi, H., *J. Mater. Sci. Lett*., 1984, **3**, 251–252.
20. Arakawa, T., Kurachi, H. and Shiokawa, J., *J. Mater. Sci*., 1985, **4**, 1207–1210.
21. Yu, C., Shimizu, Y. and Arai, H., *Chem. Lett*., 1986, 563–566
22. Post, M. L., Sanders, B. W. and Kennepohl, P., *Sensors and Actuators B*, 1993, **13**, 272–275.
23. Carotta, M. C., Butturi, M. A., Martinelli, G., Sadaoka, Y., Nunziante, P. and Traversa, E., *Sensors and Actuators B*, 1997, **44**, 590–594.
24. Carotta, M. C., Martinelli, G., Sadaoka, Y., Nunziante, P. and Traversa, E., *Sensors and Actuators B*, 1998, **48**, 270–276.
25. Matsuura, Y., Matsushima, S., Sakamoto, M. and Sadaoka, Y., *J. Mater. Chem*., 1993, **3**, 767–769.
26. Traversa, E., Matsushima, S., Okada, G., Sadaoka, Y., Sakai, Y. and Watanabe, K., *Sensors and Actuators B*, 1995, **25**, 661–664.
27. Traversa, E., Villanti, S., Gusmano, G., Aono, H. and Sadaoka, Y., *J. Am. Ceram. Soc*., 1999, **82**, 2442–2450.
28. Martinelli, G., Carotta, M. C., Traversa, E. and Ghiotti, G., *MRS Bull*., 1999, **24**(6), 30–36.
29. Martinelli, G., Carotta, M. C., Ferroni, M., Sadaoka, Y. and Traversa, E., *Sensors and Actuators B*, 1999, **55**, 99–110.
30. Traversa, E., Nunziante, P., Sangaletti, L., Allieri, B., Depero, L. E., Aono, H. and Sadaoka, Y., *J. Am. Ceram. Soc*., 2000, **83**, 1087–1092
31. Traversa, E., Sakamoto, M. and Sadaoka, Y., *Particulate Sci. Technol*., 1998, **16**, 185–214.
32. Marezio, M., Remeika, J. P. and Dernier, P. D., *Acta Cryst*., 1970, **B26**, 2008–2022.
33. Cerius^2 is distributed by Molecular Simulations/Biosym.
34. ICSD, Inorganic Crystal Structure Database, Fachinformationszentrum Karlsruhe — Gmelin Institut, Release 98/2.
35. Shannon, R. D. and Prewitt, C. T., *Acta Cryst*., 1969, **B25**, 925–946.
36. Shannon, R. D. and Prewitt, C. T., *Acta Cryst*., 1970, **B26**, 1046–1048.
37. Marezio, M. and Dernier, P. D., *Mater. Res. Bull*., 1971, **6**, 23–30.
38. Rearick, T. M., Catchen, G. L. and Adams, J. M., *Phys. Rev. B*, 1993, **48**, 224–238.